frontiers | Frontiers in Earth Science

TYPE Original Research
PUBLISHED 07 October 2024
DOI 10.3389/feart.2024.1368328

Check for updates

OPEN ACCESS

EDITED BY
Ramanathan Alagappan,
Jawaharlal Nehru University, India

REVIEWED BY
Marco Taussi,
University of Urbino Carlo Bo, Italy
Atulya Kumar Mohanty,
National Geophysical Research Institute (CSIR), India

*CORRESPONDENCE
Xiang Zhou,
zhouxiang_cnpc@163.com

RECEIVED 10 January 2024
ACCEPTED 16 September 2024
PUBLISHED 07 October 2024

CITATION
Song J and Zhou X (2024) Hydrochemical characterization and health risk assessment of shallow groundwater in a northern coalfield of Anhui Province, China.
Front. Earth Sci. 12:1368328.
doi: 10.3389/feart.2024.1368328

COPYRIGHT
© 2024 Song and Zhou. This is an open-access article distributed under the terms of the Creative Commons Attribution License (CC BY). The use, distribution or reproduction in other forums is permitted, provided the original author(s) and the copyright owner(s) are credited and that the original publication in this journal is cited, in accordance with accepted academic practice. No use, distribution or reproduction is permitted which does not comply with these terms.

Hydrochemical characterization and health risk assessment of shallow groundwater in a northern coalfield of Anhui Province, China

Jiageng Song[1] and Xiang Zhou[2]*

[1]University of Southampton, University Road, Southampton, United Kingdom, [2]Sino-Pipeline International Company, PetroChina Science and Technology Park, Beijing, China

In a global context, the hydrochemical characteristics of shallow groundwater in coalfields exhibit high degrees of diversity and complexity that are rooted in the intricate interplay of geological variations, diverse climatic conditions, and extensive human activities. The specific types and concentrations of ions, such as Ca^{2+}, Cl^{-}, and NO_3^{-}, show stark differences across geographical regions. Given the crucial roles of coalfields as energy suppliers, the potential environmental contamination risks posed by mining activities to groundwater cannot be overlooked as such pollution directly impacts human health and ecological safety. This study focuses on the Huainan coal mining area in northern Anhui Province (China), where shallow groundwater samples were systematically collected and analyzed to determine the hydrochemical characteristics and ascertain the water quality status. By integrating hydrogeochemical analysis techniques with inverse modeling methods, it was revealed that the groundwater in this region is predominantly HCO_3-Ca type, exhibiting weak alkaline characteristics. The formation mechanisms are primarily governed by silicate rock weathering and mineral dissolution–precipitation processes, albeit with discernible influences from human activities. PHREEQC simulations were used to further confirm the precipitation tendencies of minerals like calcite, dolomite, and fluorite as well as the significant dissolution characteristics of halite. The inverse modeling pathway analysis reveals specific hydrochemical processes along different paths: paths I and IV are notably dominated by Ca^{2+} dissolution–precipitation and cation exchange–adsorption processes, whereas paths II and III are closely associated with the precipitation of calcium montmorillonite as well as dissolution of kaolinite, calcite, quartz, and mineral incongruents. Moreover, evaluations based on the entropy-weighted water quality index (EWQI) indicated overall positive trends of the groundwater quality indicators within the Huainan mining area, reflecting the effectiveness of regional water quality management efforts and providing a scientific basis for future water quality protection and improvement strategies. In summary, this study not only deepens our understanding of the groundwater chemistry in the Huainan coal mining area but also underscores the importance of scientifically assessing and managing

groundwater resources to address the environmental challenges potentially arising from coal mining activities.

KEYWORDS

entropy-weighted water quality index (EWQI), health risk assessment, hydrochemistry, water–rock interactions, inverse modeling

1 Introduction

Given the increasingly vital backdrop of global environmental protection and sustainable development, the examination of shallow coalfield groundwater, specifically the global distribution patterns of its hydrochemical characteristics and objective assessments of its potential health risks, has emerged as an important topic in scientific research and policy planning (Mondal et al., 2021). Scholars acknowledge that a profound understanding of the causative mechanisms underlying the hydrochemical properties of shallow coalfield groundwater, encompassing the intricate interplay between geological formations, climatic conditions, and human activities, serves as a cornerstone for understanding and predicting the dynamic changes in groundwater quality (Tomiyama and Igarashi, 2022; Ambade et al., 2021; Prathap and Chakraborty, 2019). Detailed analyses of how industrial activities like coal mining directly impact the chemical composition of groundwater, particularly in terms of tracing the migration and transformation pathways of pollutants within the aquifer environment, are instrumental in constructing scientifically sound environmental management systems. This not only facilitates the identification of potential environmental threats but also provides a theoretical foundation for the formulation of targeted pollution prevention and control measures. Considering the invaluable status of groundwater as a natural resource underpinning the activities of daily human life and economic development, the status of its water quality is intimately tied to public health and sustainable advancements of society and the economy (Kim et al., 2021). Thus, objective and comprehensive evaluations of the health risks posed by contaminants in groundwater resources are imperative, with a particular emphasis on the health effects arising from long-term low-concentration exposure.

Evaluation of groundwater quality is pivotal for comprehending its current pollution status and assessing water-quality-related health risks. The quality of groundwater is intricately tied to geological and environmental factors, including the water source, aquifer lithology, hydrogeological characteristics, water–rock interactions, as well as evaporation and concentration processes (Xiao et al., 2021; Wu et al., 2020a; Khan et al., 2021a; Olea-Olea et al., 2024; El Ghali et al., 2020). Additionally, notable human endeavors like agricultural and industrial activities significantly impact the groundwater quality, restricting its utilization potential (Ambade et al., 2021; Rashid et al., 2022; Sahoo and Khaoash, 2020; Zipper and Skousen, 2021). Hence, deciphering the dual influences of geological conditions and human-induced factors on the chemistry of groundwater is imperative for accurate assessment of groundwater quality. Currently, the prevailing approach involves an integrated methodology of hydrogeological considerations, hydrogeochemical theories, and impacts of human activities. This holistic approach leverages statistics, the Piper diagram, the Gibbs model, the Na-end member diagram, isotopic analyses, as well as ion correlation and ratio coefficient methods to uncover the controlling factors and origins of the hydrochemical constituents (Fan et al., 2014; Yan et al., 2021; Li et al., 2020; Li et al., 2019a). By employing this multifaceted strategy, we can gain a more profound understanding of groundwater quality and its dynamics.

The Huainan mine is strategically positioned in the eastern sector of the expansive Huainan coalfield in Anhui Province and boasts a vast mine boundary extending eastward, embracing the terrain adjacent to the southern bank of the Huai River (China) (Figure 1A). The figure not only pinpoints the distribution of the sampling sites but also shows the directional flow of surface water runoff and extensive coverage of the Quaternary unconsolidated layer within the region. To delve into the environmental geological landscape of this site, we consider the FS130 sampling point shown in Figure 1B as a representative case study. Groundwater is a vital lifeline water supply for the mining area; it has been increasingly threatened by pollution amid the intensifying industrial, agricultural, and mining activities in its vicinity. In the context of the Huaibei Plain, aquifer depths are categorically defined as shallow (less than 30 m), medium (30–50 m), and deep (exceeding 50 m). Notably, current groundwater research in the Huainan coal mine area is predominantly focused on the intricate deep groundwater system; Wang et al. (2019) reported a comprehensive analysis of the water chemistry in major outburst aquifers across 16 mines, elucidating the spatial distribution patterns and aquifer functionalities. Similarly, Huang et al. (2020) explored the compositional nuances and evolutionary traits of sandstone and ash water in the Xinji mining area, revealing key water–rock interactions involving silicate and evaporite dissolution along with cation adsorption dynamics. However, a notable gap exists in our understanding of the hydrochemical evolution mechanisms specific to shallow groundwater in the Huainan mining area as well as the associated health risks posed by contaminated groundwater. This gap underscores the urgency for targeted research endeavors that not only unravel the intricacies of shallow groundwater chemistry but also assess and mitigate the potential health hazards, thereby safeguarding the wellbeing of communities reliant on these vital water resources.

In light of the aforementioned considerations, this study considers the Huainan coal mine as the focal point for exhaustive analyses of the groundwater hydrochemical attributes. Drawing upon these analyses, we delve into the origins of groundwater quality degradation within the study area using both hydrogeochemical simulation and hydrochemical mapping techniques. Our efforts also include a rigorous water quality assessment that pinpoints the pivotal indicators contributing to the decline in groundwater quality. Furthermore, we report a health risk evaluation specifically tailored to these key indicators by considering both dermal exposure and direct ingestion routes.

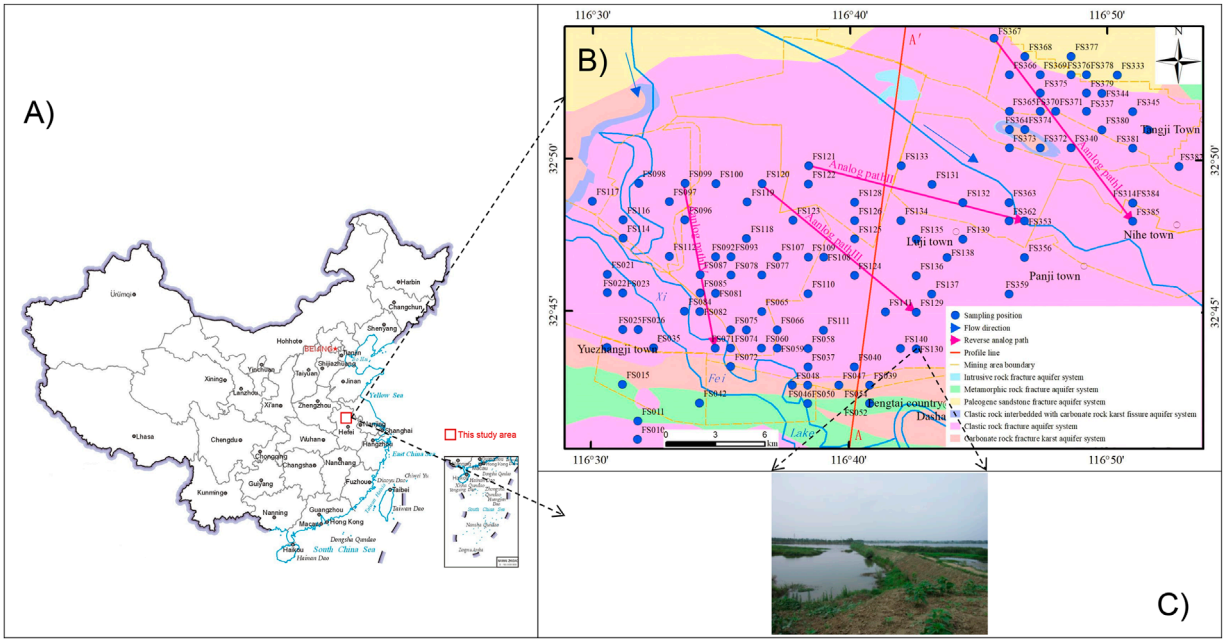

FIGURE 1
(A) Map of China showing the **(B)** geology of the study area along with the locations of the sampling points, direction of water flow, mining area boundaries, and other element information; **(C)** geomorphic map of the sampling point FS130.

The objectives of this study are structured to address the following intricate facets. (1) Comprehensive hydrochemical characterization of shallow groundwater: we meticulously examine the hydrochemical signatures of the shallow groundwater in the Huainan coal mining region to provide a foundational understanding of its chemical makeup. (2) Inverse hydrogeochemical simulation for evolutionary insights: by employing advanced simulation techniques, we reconstruct the evolutionary trajectory of the groundwater components to offer invaluable insights into their historical transformations and current status. (3) Entropy-weighted water quality index (EWQI) assessment: by leveraging the EWQI framework, we evaluate the groundwater quality objectively to ensure a comprehensive and scientifically rigorous assessment capturing the multifaceted nature of the water quality parameters. (4) Health risk assessment model for real-world exposures: by acknowledging the dire consequences of groundwater contamination on public health, we present a robust health risk assessment framework incorporating exposure pathways pertinent to the study region, including skin contact and direct ingestion, thereby enabling precise quantification of the potential health hazards in a manner that informs actionable strategies.

2 Overview of the study area

The research area is located in the northern part of Anhui Province, to the north of the middle and lower reaches of the Huai River (western section of Fengtai County, Huainan City, Eastern China). The region is an alluvial plain of the Huaihe River, with a flat terrain that gradually slopes from northwest to southeast, and a ground elevation of 15.5–25 m (Chai, 2018). The Huainan coal mine area is located in the north–south climate transition zone of China, with an annual average temperature of 11–14°C, a seasonal average rainfall of 600–1,400 mm (600 mm: dry season, November to April of the following year; 1400 mm: wet season, May to October), and an annual average evaporation of 800–1,200 mm (Chai, 2018). The surface water body in the area is developed, and the larger rivers are mainly the Huaihe River and its tributaries (Yinghe River, Ni River, Xihe River, Xifei River, and Heihe River).

There are 12 kinds of mineral energy sources, including coal, coal bed methane, and geothermal energy, as well as non-metallic mineral resources, such as limestone, dolomite, kaolin, and chemical mineral resources. The strata belong to the Huainan Formation area in the Xuhuai Formation area of Shanxi–Hebei–Shandong–Henan, North China Formation Region. With the exception of the Middle Cenozoic, Silurian, Devonian, Carboniferous, and Triassic, the different mineral resources mentioned above are found in varying degrees within the strata of other eras. However, the overall scale of mineralization remains limited (Huang et al., 2020; Chai, 2018).

The different aquifer systems in the study area include loose rock pore water content system, carbonate rock fissure karst water content system, and debris rock pore fissure water content system (Figure 2). The loose rock pore water content system is composed of Quaternary and Neogene loose deposits; the carbonate rock karst water content system is composed of Cambrian, Ordovician, and Carboniferous carbonatites; the debris rock pore fissure water content system is composed of carboniferous rock, sandstone, and shale, among others (Huang et al., 2020; Chai, 2018). Here, the groundwater receives atmospheric replenishment, and Huaihe River is the lowest discharge point.

The thickness of the loose layer in the mining area is generally 250–450 m, with the maximum thickness being 700 m.

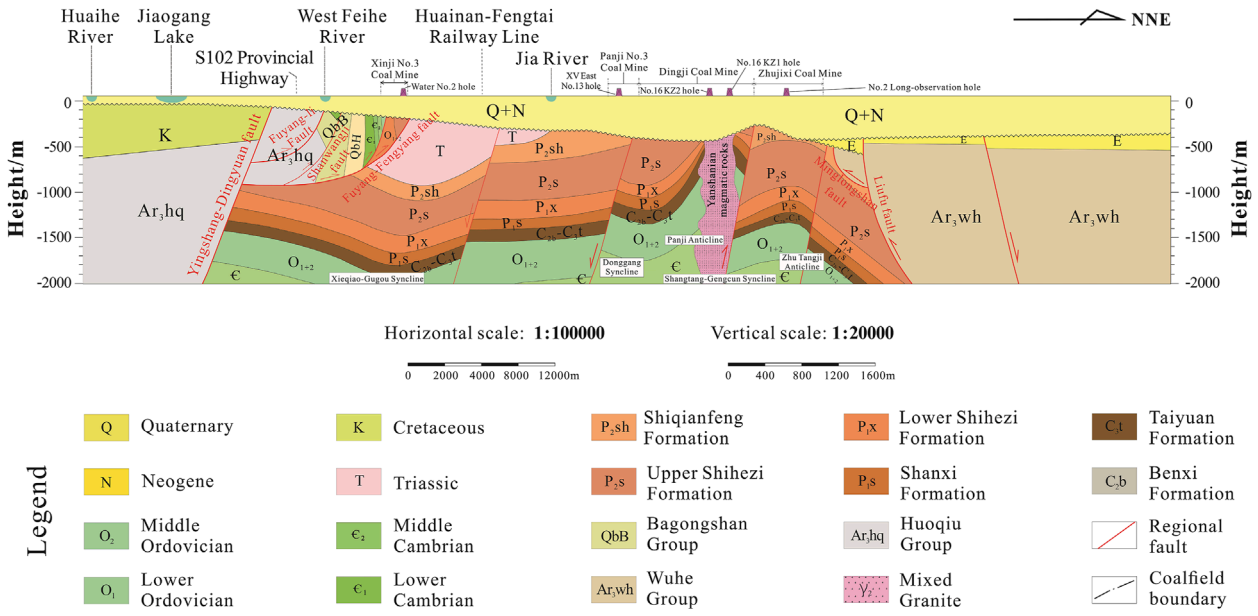

FIGURE 2
Geological profile corresponding to the A-A′ line in Figure 1.

The distribution on the plane is uneven, and the thickness gradually increases from south to north and east to west. The loose rock pore water aquifer can be divided into four aquifer groups and four aquiclude groups from top to bottom. The lithology of the aquifer group is silty sand and fine sand, and the water yield of the water-rich single well is 500–1,000 m^3 d^{-1}. The aquicludes are composed of clayey soil deposited in the Late Pleistocene and Pliocene of Neogene; their lithology is mainly clay and loam, partially semi-cemented, with a general thickness of 30–50 m; the clayey soil has a compact structure and extremely poor permeability, with a general permeability coefficient of 1×10^{-6}. The carbonate fissure karst water mainly exists in the Paleozoic and Upper Proterozoic carbonate karst fissures, and the lithology of the water-bearing formation is limestone, dolomitic limestone, and calcareous dolomite (Yang et al., 2021). The water abundance is poor, and the water inflow of a single well is generally less than 500 m^3 d^{-1}. The clastic rock pore and fissure water mainly exists in the pores and fissures of the clastic rocks of the Lower Tertiary, Mesozoic, Paleozoic, and Upper Proterozoic, and the lithology of the water-bearing formation includes sandstone, shale, and mudstone, among others. The water abundance is controlled by the structure, and the groundwater is unevenly distributed. The water abundances of the coal measure formation lime and Permian clastic rock are generally poor, and the water inflow of a single well is generally less than 100 m^3 d^{-1}. Bedrock fracture water is mainly found in the weathering fractures of the metamorphic rocks of the Lower and Upper Paleozoic, and the lithology of the water-bearing rock groups includes marble, black cloud dioritic gneiss, mixed rock, and mixed granite with dioritic hornblende. The water richness is poor and water inflows of the individual wells are less than 100 m^3 d^{-1} (Wu et al., 2022). The groundwater receives atmospheric recharge, and the Huaihe River is the lowest discharge point.

3 Materials and methods

3.1 Sample collection and testing

From October to November 2016, shallow groundwater samples were collected around Fengtai County of the Huainan coal mine area for a total of 110 sets of water samples (Figure 1). The shallow groundwater samples were taken from small distributed rural water supply wells, farmland irrigation machine wells, and drilling holes around the mining area at depths between 7 and 50 m. Parameters such as the pH and total dissolved solids were measured at each collection site using the SD150 portable multiparameter water quality tester. Each group of samples was collected in two polyethylene plastic bottles and washed with ionic water at least three times; one of the bottles containing the water sample had a volume of 500 mL, to which 1:1 nitric acid solution was added at pH <2 to determine the sample cation concentration; the other bottle had a volume of 1,000 mL, which was retained without treatment to determine the sample anion concentration. The water samples were sent to the Hefei Mineral Resources Supervision and Testing Center of the Ministry of Land and Resources within 24 h of collection for testing.

The ion chromatograph (Thermo Dionex, ICS-2500, USA) was used to test the concentrations of SO_4^{2-}, Cl^-, F^-, and NO_3^- in the samples. The baseline noise was 0.01 μs, and the minimum detection limit was ≤0.04 mg L^{-1}. The concentration of H_2SiO_3 in the samples was measured using a 722N spectrophotometer (Shanghai Metash Instruments Co., Ltd). The SO_4^{2-}, Cl^-, and NO_3^- concentrations were determined with the Dionex-2500 ion chromatograph, and the K^+, Na^+, Ca^{2+}, and Mg^{2+} concentrations were determined with the ICAP 6300 inductance coupled plasma spectrometer. The HCO_3^- concentration was determined by titration. The limit of detection of each ion was 0.01 mg L^{-1}, and the measurement errors of the anions

and cations were generally lower than 0.1%. The parameter analysis errors were tested using the cation–anion concentration balance method and the following test equation:

$$E = \frac{\sum m_c - \sum m_a}{\sum m_c + \sum m_a} \times 100, \quad (1)$$

where E is the relative error in %; m_c is the cation milligram equivalent concentration in meq L^{-1}; m_a is the anion milligram equivalent concentration in meq L^{-1}.

3.2 Groundwater quality evaluation

The EWQI is a modification of the traditional water quality index (WQI) and is currently widely used in the evaluation of regional groundwater quality (Mondal et al., 2021; Wu et al., 2022; Ukah et al., 2020; Kumar and Augustine, 2022). The specific calculation steps are as follows (Mondal et al., 2021; Du et al., 2022):

(1) Construct the characteristic parameter matrix of the water chemical components X as

$$X = \begin{bmatrix} x_{11} & x_{12} \cdots & x_{1n} \\ x_{21} & x_{22} \cdots & x_{2n} \\ \vdots & \vdots \ x_{ij} & \vdots \\ x_{m1} & x_{m2} \cdots & x_{mn} \end{bmatrix}. \quad (2)$$

(2) Determine the normalized parameter matrix Y as

$$y_{ij} = \frac{x_{ij} - (x_{ij})_{min}}{(x_{ij})_{max} - (x_{ij})_{min}}. \quad (3)$$

$$Y = \begin{bmatrix} y_{11} & y_{12} \cdots & y_{1n} \\ y_{21} & x_{22} \cdots & y_{2n} \\ \vdots & \vdots \ y_{ij} & \vdots \\ y_{m1} & y_{m2} \cdots & y_{mn} \end{bmatrix}. \quad (4)$$

(3) Calculate the ratio P_{ij} and information entropy E_j of the parameters:

$$P_{ij} = \frac{y_{ij}}{\sum_{i=1}^{m} y_{ij}}. \quad (5)$$

$$E_j = \frac{1}{\ln m} \times \sum_{i=1}^{m} P_{ij} \ln P_{ij}. \quad (6)$$

(4) Calculate the information entropy weight ω_j and groundwater quality grade q_j:

$$\omega_j = \frac{1 - E_j}{\sum_{i=1}^{n} (1 - E_j)}. \quad (7)$$

TABLE 1 Classifications of the EWQI.

EWQI	Grade	Classification
EWQI<25	1	Excellent
25≤EWQI<50	2	Good
50≤EWQI<100	3	Medium
100≤EWQI<150	4	Poor
EWQI≥150	5	Bad

$$q_j = \frac{C_j}{S_j} \times 100. \quad (8)$$

(5) Determine the EWQI as

$$\mathrm{EWQI} = \sum_{j=1}^{n} \omega_j q_j. \quad (9)$$

Here, m is the number of water samples, n is the selected water chemical component parameter, and x_{ij} is the jth parameter of the ith sample; Cj is the concentration of each chemical component in each water sample in mg L^{-1}; Sj is the parameter limit specified by the World Health Organization or national standards in mg L^{-1}. The groundwater quality was then divided into five grades based on the EWQI values that can be calculated using Equations 1–9 (Table 1) (Mondal et al., 2021).

3.3 Health risk assessment

The human health risk assessment model built by the US Environmental Protection Agency (USEPA) is widely used to assess the potential harmful effects of groundwater pollutants on child and adult health (Gao et al., 2020; Liu et al., 2022). The harmful substances in the groundwater environment can be divided into non-chemical and chemical carcinogens, and their exposure route is mainly through drinking water intake or skin contact (Mondal et al., 2021; Gao et al., 2020; Liu et al., 2022; Wu et al., 2020b). Thus, the following calculations are made:

$$CDI_i = \frac{C_i \times \mathrm{IR} \times \mathrm{ABS} \times \mathrm{EF} \times \mathrm{ED},}{\mathrm{BW} \times \mathrm{AT}} \quad (10)$$

$$CDD_i = \frac{C_i \times \mathrm{SA} \times \mathrm{KP} \times \mathrm{EV} \times \mathrm{ED} \times \mathrm{CF}}{\mathrm{BW} \times \mathrm{AT}}, \quad (11)$$

$$\mathrm{HQ}_i = \frac{CDI_i (CDD_i)}{RfD}, \quad (12)$$

$$\mathrm{HI} = \sum_{i=1}^{n} \mathrm{HQ}_i, \quad (13)$$

where CDI is the drinking water intake in mg kg^{-1} d^{-1}; CDD is the contact exposure dose in mg kg^{-1} d^{-1}; HQ is the risk of non-carcinogenic pollutants in a certain exposure route; HI is the total

TABLE 2 Parameters employed for human health risk assessments.

Parameter name		Unit	Children	Female	Male
IR	Drinking water rate	L d^{-1}	1.8	2.66	3.62
BW	Average weight	kg	30	50	65
ET	Bath time	h d^{-1}	0.3	0.5	0.2
ABS	Gastrointestinal absorption coefficient	Non-dimensional	0.5	0.5	0.5
AT	Average exposure time	d	365×ED	365×ED	365×ED
EV	Bath frequency	Non-dimensional	1.5	1	2
KP	Skin permeability coefficient	cm h^{-1}	0.001	0.001	0.001
CF	Volume conversion factor	L cm^{-1}	0.001	0.001	0.001
ED	Exposure duration	a	12	30	30
EF	Exposure frequency	d a^{-1}	365	365	365
SA	Skin contact area	cm^2	1.20×10^5	1.50×10^5	1.60×10^5
RfD	Nitrate reference dose	mg kg^{-1} d^{-1}	1.6	1.6	1.6

non-carcinogenic health risk index (non-dimensional); RfD is the reference concentration of contaminants in groundwater in mg kg^{-1} d^{-1}. The specific values of the other parameters used are as shown in Table 2 (Wu et al., 2022; Zhang et al., 2018). Considering the different physiological states of people in different age and gender groups, the drinking water population in the study area for health risk assessment was divided into children, adult men, and adult women. When HI(HQ) <1, the non-carcinogenic health risk caused by pollution is within a controllable range; when HI(HQ) >1, the non-carcinogenic health risk caused by pollution is uncontrollable. As the HI value obtained from Equations 11–13 increases, the non-carcinogenic risk increases correspondingly.

3.4 Data processing

ArcGIS10.8 software was used to obtain the distribution map of the groundwater sampling points, and a multivariate statistical analysis of the groundwater hydrochemical data was carried out using SPSS 26.0; further, Origin 2021 was used to draw the relevant maps. PHREEQC software was used to calculate the saturation index of the hydrochemical components and perform the inverse hydrogeochemical simulation.

4 Results

4.1 Hydrochemical characteristics

The main statistical indicators of the groundwater in the study area are shown in Table 1. The pH of the groundwater in the study area was between 7.27 and 8.26, with a mean value of 7.74, which is weakly alkaline as a whole. According to GB 5749-2022 (standards for drinking water quality), water is classified according to the value of the total dissolved substances (TDS). This means that if TDS is less than 1,000 mg L^{-1}, it is freshwater; if TDS is more than 1,000 mg L^{-1}, it is brackish water; a TDS of more than 3,000 mg L^{-1} implies salt water. In the study area, the TDS was between 204.98 and 1,278.12 mg L^{-1}, with an average value of 568.75 mg L^{-1} (Table 3), indicating freshwater. The concentrations of the solute components were in the order of HCO_3^- > Ca^{2+} > Cl^- > Na^+ > SO_4^{2-}> H_2SiO_3 > Mg^{2+} > NO_3^- > K^+. The main anion was HCO_3^- that accounted for 75.22% of the anion concentration, followed by Cl^- and SO_4^{2-}; the main cation was Ca^{2+} with a concentration of 51.47%, followed by Na^+. In this study, the concentration of metasilicic acid (H_2SiO_3) was mainly used to extrapolate the SiO_2 content of the water samples for the inverse hydrogeochemical modeling.

The coefficient of variation of the main ions in the groundwater ranges from 0.23 to 1.68 with large spatial variations. The variation coefficients of K^+, Cl^-, SO_4^{2-}, and NO_3^- all exceed 1, indicating clear differential spatial distribution and high degrees of local ion enrichment that may be affected by human activities (Khan et al., 2021a; Zhang et al., 2014). Related studies have shown that nitric acid water formation is mainly affected by human domestic sewage, agricultural fertilization, septic tank, and landfill leach infiltration (Bakshe et al., 2024; Meng, 2021); this indicates that the groundwater in the study area was affected by human activities.

The Piper diagram shows that there are no effects from human factors and directly reflects the type and evolution characteristics of groundwater hydrochemistry (Piper, 1944; Addis, 2023). According to Figure 3, HCO_3^- and SO_4^{2-} are the main anions, while Ca^{2+} and Na^+ are the main cations in the study area, indicating that the water bodies in the area had medium or above levels of salinity. The main cations in the groundwater are Ca^{2+}, Na^+, and

TABLE 3 Hydrochemical statistical characteristics of groundwater in the study area.

Type	Project	pH	TDS	K^+	Na^+	Ca^{2+}	Mg^{2+}	Cl^-	SO_4^{2-}	HCO_3^-	NO_3^-	H_2SiO_3
Underground water n=110	Max	8.26	1,278.12	5.81	212.10	235.87	65.99	268.00	191.16	592.50	180.97	52.38
	Min	7.27	204.98	0.12	15.00	35.73	6.83	1.06	0.00	186.21	0.50	15.63
	Mean	7.74	568.75	0.59	56.71	89.88	23.10	63.06	31.51	368.43	18.83	24.50
	Std	0.20	209.06	0.69	36.48	38.01	11.01	64.34	38.07	85.34	31.67	4.35
	Cv/%	0.03	0.37	1.16	0.64	0.42	0.48	1.02	1.21	0.23	1.68	0.18
Guidance value (Groundwater quality standard, 2017; WHO, 2011)		6.5–8.5	1,000	200	200	75	50	250	250	—	50	—

Max represents the maximum value; Min is the minimum value; Mean is the mean value; Std is the standard deviation; Cv is the coefficient of variation; pH is dimensionless, and all other components are in mg L^{-1}.

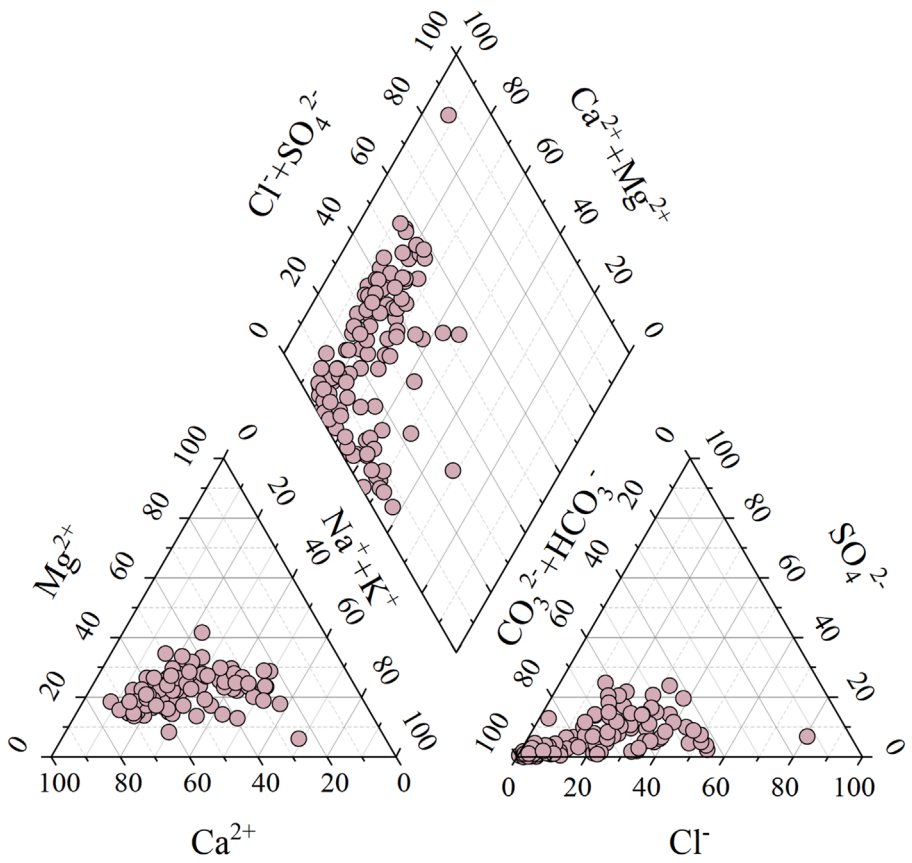

FIGURE 3
Piper diagram of groundwater chemistry.

Mg^{2+}. Based on this finding, it is speculated that the cations in the groundwater mainly came from weathering and dissolution of carbonate, silicate, and evaporite rocks.

There were various types of groundwater in the study area. According to Shukarev's classification (Aliejin, 1960), the groundwater was mainly HCO_3-Ca water, accounting for 32.17%, followed by HCO_3-Ca·Na (21.74%), HCO_3.Cl-Ca (13.04%), and HCO_3-Ca·Na·Mg (9.57%); the hydrochemical type of the groundwater gradually evolved as Cl-Ca·Na → HCO_3-Ca·Mg → HCO_3-Na. The water–rock interactions between groundwater and the surrounding media cause changes in the chemical components of the groundwater (Gibbs, 1970); such water–rock interactions

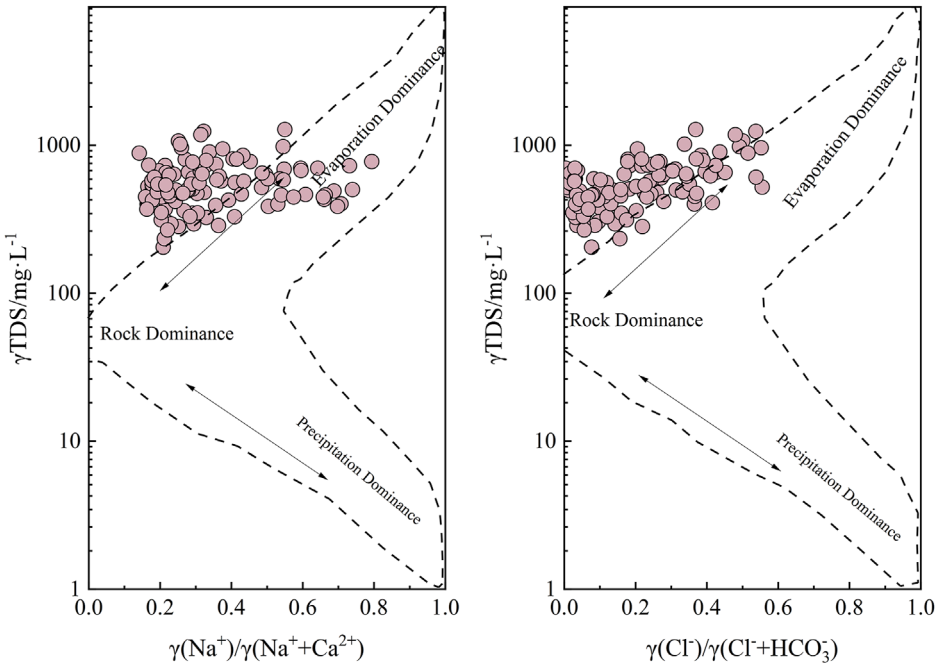

FIGURE 4
Gibbs diagram of groundwater in the study area.

can reveal the mechanisms of hydrochemical evolution. Gibbs plots can be used to qualitatively determine the effects of atmospheric rainfall, rock weathering, and evaporation concentration on the groundwater ion sources (Gibbs, 1970; Li et al., 2019b; Andres and Paul, 2018).

As shown in Figure 4, the cationic $\gamma(Na^{+})/\gamma(Na^{+}+Ca^{2+})$ was between 0.14 and 0.89, and the anionic $\gamma(Cl^{-})/\gamma(Cl^{-}+HCO_3^{-})$ was between 0.01 and 0.65. The groundwater samples mostly indicate end elements from water–rock interactions (rock weathering control), meaning that such interactions dominate the hydrogeochemical processes in the research area. The groundwater hydrogeochemical characteristics also indicated that most of the samples contained evaporation–concentration end elements, but these were far lower than those from water–rock interactions. The distribution of the sample points was far from the rainfall control element, indicating that atmospheric precipitation contributed less to the main sources of ions in the groundwater in the study area.

The amounts and concentration ratios of Mg^{2+}/Na^{+}, Ca^{2+}/Na^{+}, and HCO_3^{-}/Na^{+} produced by weathering of carbonate, silicate, and evaporite minerals were significantly different, which could qualitatively determine the influences of weathering and dissolution of different types of rocks on the groundwater solutes (Bakshe et al., 2024; Gaillardet et al., 1999). The groundwater sampling points in the study area were mainly distributed near the silicate rock terminal area (Figure 5), with only a few sampling points near the evaporite end, and the sampling points trended toward the carbonate rock area. This shows that weathering hydrolysis of silicate minerals (such as feldspar) controls the hydrogeochemical processes in the study area; however, the contributions of the evaporite minerals cannot be excluded.

4.2 Hydrogeochemical simulation

Hydrogeochemical simulations are an important method to study the chemical roles of groundwater. The commonly used procedures here are the saturation index and mass balance simulations that are then used to perform the inverse hydrogeochemical simulation (Liu et al., 2019). The saturation index (SI) is an important indicator of the hydrogeochemical characteristics of groundwater and is defined as follows:

$$SI = \lg \frac{IAP}{K}, \tag{14}$$

where IAP is the activity product of the related ions in the mineral dissolution reaction, and K is the equilibrium constant of the mineral dissolution reaction at a certain temperature. When SI = 0, the mineral dissolution is in equilibrium; when SI > 0, the minerals are oversaturated and precipitated; when SI < 0, the minerals are undersaturated and dissolved.

The mass balance simulation is used to mainly study the chemical reactions in the groundwater flow path. Given two hydrochemical samples in the water flow path, the mass balance simulation is used to quantitatively explain the chemical reactions and changes between the groundwater and water-containing medium as well as determine the dissolution or precipitation of minerals during groundwater flow.

4.2.1 Saturation index

In the study area, the SI of calcite in the water samples based on Equation 14 was between 2.76 and 3.52, with an average value of 3.18; the SI of dolomite was between 4.88 and 6.85, with an average value of 5.91. The SI values of the above two minerals were greater

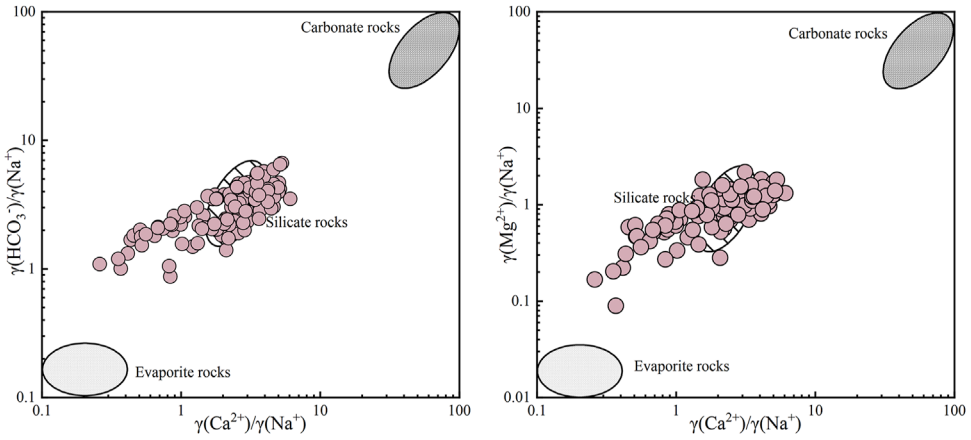

FIGURE 5
Relationships between HCO_3^-/Na^+, Mg^{2+}/Na^+, and Ca^{2+}/Na^+ in the groundwater.

than 0, indicating that calcite and dolomite were supersaturated in the study area, which enabled precipitation and generation of the precipitate crystals. The SI of fluorite was between −0.63 and 2.36, with a mean value of 1.02; the SIs of only five samples were below 0, indicating that fluorite was supersaturated in the study area and was prone to precipitation. The SI of halite was between −6.06 and −3.33, with a mean value of −4.72; the SIs of halite in all samples were less than 0, which indicated that halite was undersaturated in the study area and that it continuously dissolved into the shallow groundwater. The SI of gypsum was between −1.88 and 1.07, with a mean of −0.13, indicating that the groundwater gypsum content generally tended to equilibrium (Figure 6A).

The SI values of calcite, dolomite, and fluorite in the shallow groundwater were mutually independent of the TDS (Figures 6B–D). Related studies have shown that carbonate rocks are prevalent in aquifers in the zone (Wu et al., 2022; Liu et al., 2019). Although both calcite and dolomite were saturated, carbonate rocks were likely to dissolve rapidly during the initial stages of the chemical evolution of the groundwater (Zineb and Meriem, 2024). Therefore, carbonate dissolution was considered an important source of HCO_3^-, Ca^{2+}, and Mg^{2+} in the shallow groundwater of the study area. The Huainan coal mine area is located in the south of the Huaibei Plain, and Xu et al. (2009) reported that the concentration of F in the groundwater of the Huaibei Plain exceeded the Chinese standard value (GB 5749-2022 "Standards for drinking water quality") by 23%, implying that the groundwater in the study area has a high F concentration. The continuous dissolution of fluoride minerals is one of the main reasons for fluoride ion enrichment of the shallow groundwater. However, the SIs of fluorite in the groundwater samples exceeded 0 and calcium content of the shallow clay minerals was high, which was beneficial for the fluoride and calcium ions to form CaF_2 (Xu et al., 2009). The SIs of halite and gypsum in the shallow groundwater increased with the concentration of TDS (Figures 6E, F), indicating that the increase in TDS in the shallow groundwater of the Huainan coal mine was associated with the dissolution of halite and gypsum.

The CO_2 dissolved in groundwater could lead to the dissolution of many minerals, especially carbonate rocks. The CO_2 partial pressure ($LogP_{CO2}$) of shallow groundwater in the study area ranged from −1.23 to 0.00 atm, with a mean value of −0.61 atm. It is seen from Figure 7 that the value of P_{CO2} in shallow groundwater was negatively correlated with the pH value, and the pH value increased with decrease in P_{CO2} (Figure 7A). Feldspar minerals such as sodium and potassium feldspar were prevalent in the aqueous medium in the study area (Liu et al., 2019; Xu et al., 2009); feldspar-like minerals continuously consume CO_2 in the process of dissolution, which led to increased HCO_3^- ion concentration and increase in the pH value. In addition, there was a negative correlation between P_{CO2} and calcite SI (Figure 7B), and the decrease in P_{CO2} led to increase in calcite SI, indicating that CO_2 consumption promoted calcite precipitation (Zineb and Meriem, 2024).

4.2.2 Inverse hydrogeochemical simulations

According to the distribution of the sampling points and groundwater flow direction, four shallow groundwater routes in different regions of the study area were selected for inverse hydrogeochemical simulations (Figure 1). Phreeqc.dat was selected as the thermodynamic database, and the uncertainty limit was set to 5.0%. The chemical compositions of the water samples at each starting and end points on each route are shown in Table 4. Based on the hydrogeological conditions of the study area, the possible potential mineral/substance input phases were set as follows: calcium montmorillonite, kaolin, quartz, illite, dolomite, gypsum, halite, fluorite, calcite, and Ca^{2+}/Na^+ cation exchange. The results of the inverse simulated phase molar transfer for each route are shown in Table 5.

The hydrochemical evolutions varied for the simulation paths. In path I, calcium montmorillonite and gypsum were dissolved, while kaolinite, calcite, dolomite, and other minerals were generated, and halite was precipitated. The molar transfer difference of each mineral was small, which mainly manifested as ion-exchange adsorption, leading to a significant increase in Ca^{2+} and drastic decrease in Na^+ in this path. In path II, calcium montmorillonite was precipitated, while gypsum, kaolinite, calcite, halite, and quartz were dissolved, especially quartz, which was larger than the other minerals; at the same time, cation-exchange adsorption occurred

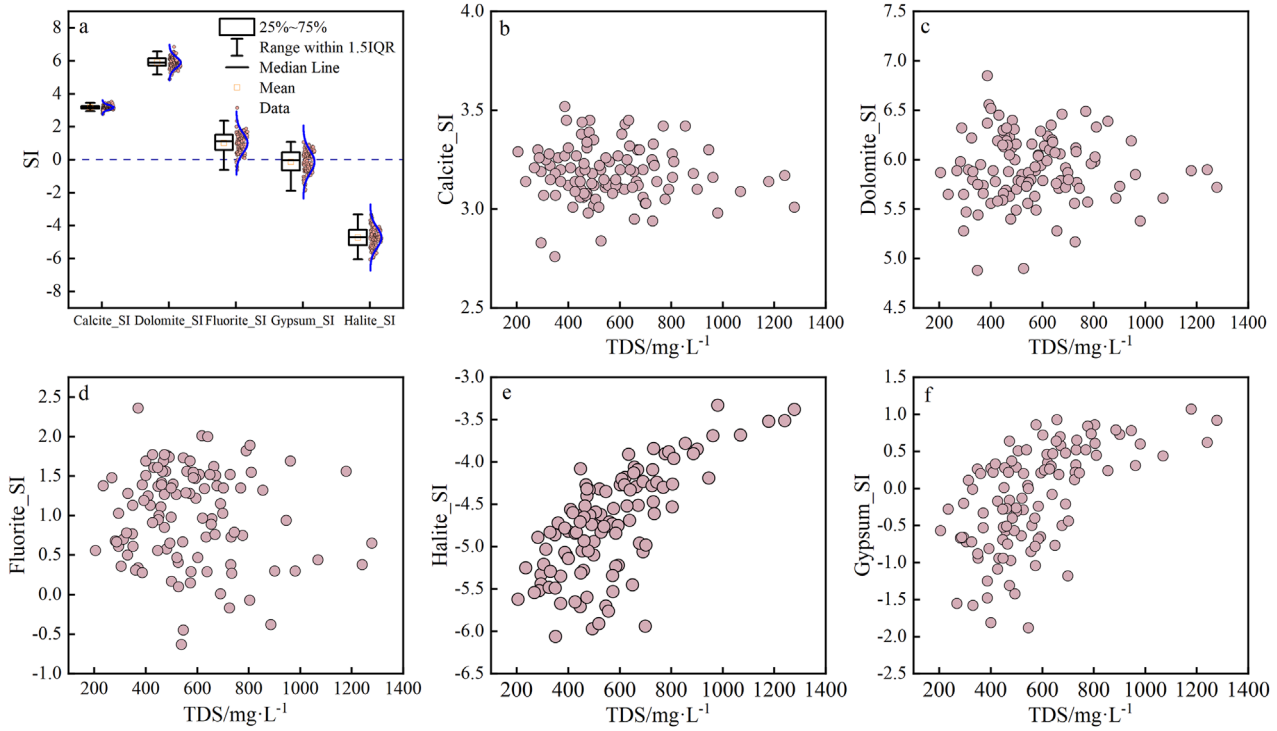

FIGURE 6
Relationships between different mineral saturation indices (SIs) and the total dissolved substances (TDS). Among them, **(A)** represents the mathematical statistical results of SI values of five minerals; **(B–F)** show the correlation between SI values and TDS of the minerals Calcite, Dolomite, Fluorite, Halite, and Gypsum respectively.

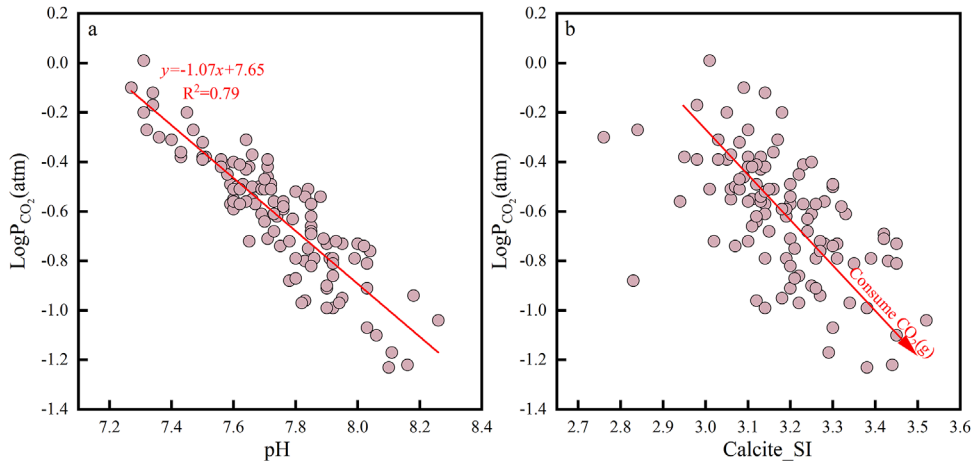

FIGURE 7
Relationships of the partial pressure of CO_2 against pH **(A)** and calcite saturation index **(B)**.

in this path, but it was not the main hydrochemical evolution. Large amounts of kaolinite and calcite were dissolved, while calcium montmorillonite was precipitated, but the rate of Ca^{2+} precipitation was far lower than that of Ca^{2+} dissolution, which led to a large increase in Ca^{2+} in the solution. The evolution of path III was generally consistent with that of path II, except that the cation exchange was different. In path III, CaX_2 was adsorbed and NaX was desorbed. The evolution process of path IV was relatively consistent with that of path I, but the main difference was that calcite was dissolved and dolomite was precipitated along this path, indicating that non-congruent dissolution occurs in this path (Samal et al., 2022). Overall, the hydrochemical evolution in the study area resulted in hydrochemical type change from HCO_3^--Ca^{2+}·Na^+ to HCO_3^--Ca^{2+}.

TABLE 4 Chemical compositions of the water samples at the start and end points of each path.

Ionic parameters	Path I (FS367→FS385)		Path II (FS121→FS362)		Path III (FS120→FS129)		Path IV (FS099→FS071)	
	Starting points	Terminal points	Starting points	Terminal points	Starting points	Terminal points	Starting points	Terminal points
pH	7.99	7.73	7.64	8.03	7.66	7.64	7.56	7.74
Na^+	99.63	29.52	92.88	46.79	85.84	35.31	45.34	26.64
K^+	0.58	0.40	0.44	0.65	0.46	0.41	0.14	0.28
Ca^{2+}	45.09	93.19	55.23	73.75	61.61	76.29	95.99	77.15
Mg^{2+}	24.55	18.86	25.05	22.48	27.27	21.38	34.15	9.72
Cl^-	69.84	49.31	1.06	14.18	8.86	4.61	49.63	10.64
HCO_3^-	404.56	294.02	522.36	437.51	487.95	406.39	388.09	331.95
SO_4^{2-}	3.84	52.82	2.00	3.36	17.06	0.24	61.96	3.36
NO_3^-	0.50	0.50	0.50	11.05	0.50	0.50	24.45	0.50
F^-	0.64	0.04	0.40	0.40	0.44	0.68	0.48	0.16
SiO_2	16.22	20.88	17.37	22.10	17.13	21.73	16.47	21.84

TABLE 5 Molar transfer for phases in different routes in mol L^{-1}.

Inverse simulation path	Calcium montmorillonite	Gypsum	Kaolinite	Calcite	Quartz	Dolomite	Halite	Fluorite	CaX_2	NaX
Path I	6.48×10^{-5}	5.10×10^{-4}	-7.32×10^{-5}	-5.02×10^{-4}	\	-3.22×10^{-4}	-5.80×10^{-4}	-1.58×10^{-5}	1.35×10^{-3}	-2.69×10^{-3}
Path II	-6.14×10^{-1}	1.45×10^{-5}	7.15×10^{-1}	1.01×10^{-1}	8.23×10^{-1}	\	3.71×10^{-4}	\	1.16×10^{-3}	-2.32×10^{-3}
Path III	-4.17×10^{1}	2.50×10^{-6}	4.86×10^{1}	6.89	5.59×10^{1}	8.80×10^{-4}	1.30×10^{-4}	1.79×10^{-5}	-7.03×10^{-4}	1.41×10^{-3}
Path IV	6.13×10^{-5}	6.11×10^{-4}	-7.32×10^{-5}	1.41×10^{-3}	\	-1.01×10^{-3}	-1.10×10^{-3}	-8.43×10^{-6}	-1.43×10^{-4}	$2.86E\times10^{-4}$

Note: a positive number indicates that the mineral is dissolved; a negative number indicates precipitation; "\" indicates no value.

5 Discussion

5.1 Analysis of groundwater quality in the study area

Ten parameters, namely, pH, TDS, Na^+, Ca^{2+}, Mg^{2+}, Cl^-, SO_4^{2-}, NO_3^-, and F^-, were selected for the EWQI evaluation. The calculation results showed that the EWQI values of the shallow groundwater samples in the study area ranged from 11.62 to 287.65, with a mean value of 48.93. According to the EWQI classification table, values less than 25 comprised 45.45%, values between 25 and 250 comprised 20.00%, values between 50 and 100 comprised 24.55%, values between 100 and 150 comprised 6.36%, and values greater than 150 comprised 3.64%. The results also showed that 65.45% of the samples in the study area were of grades 1 and 2, i.e., excellent and good grades with good chemical status; the domestic groundwater samples accounted for 24.55%, while 3.64% of the groundwater was poor quality and non-potable with grade 5 (Wu et al., 2022). As seen from Figure 8, groundwater of excellent, good, and medium grades was distributed in the entire area, while poor grade groundwater was distributed sporadically and may have been affected by point-source pollution from mining and agricultural activities (Bakshe et al., 2024).

Comparing the parameters and EWQI values, it was found that the EWQI increased significantly with increase in NO_3^- ion concentration (Figure 9A), and its correlation coefficient reached 0.98. However, the increase in F^- concentration did not lead to a significant increase in the EWQI (Figure 9B). Thus, it could be inferred that NO_3^- ions were the main cause of groundwater grade changes and the main contributors to groundwater quality change. SO_4^{2-}, Cl^-, NO_3^-, and Na^+ produced by human activities such as agricultural production and mineral exploitation control the changes to the chemical components of surface water or groundwater (Gomez and Martínez,

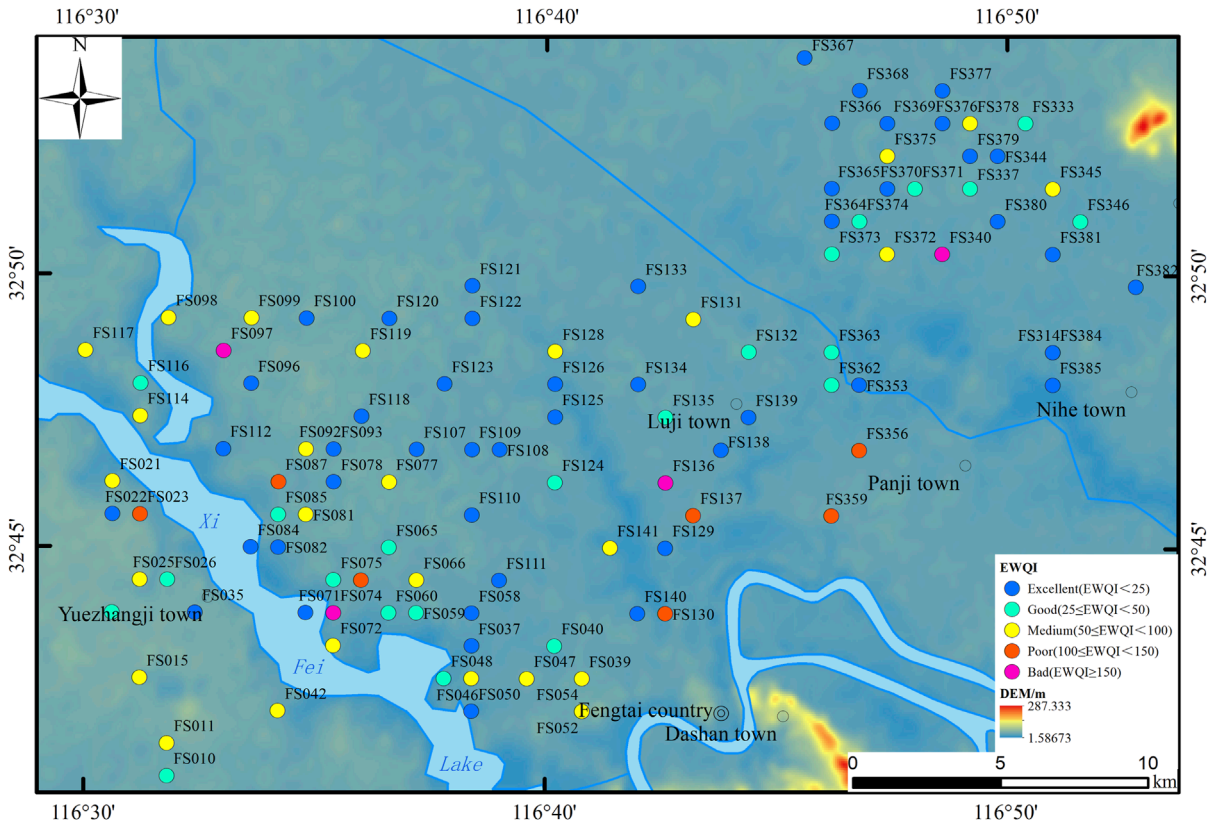

FIGURE 8
Distribution map of the groundwater quality grade in the study area.

2010). Mining activities produce more SO_4^{2-}, while agricultural production and domestic sewage discharge lead to enrichment and migration of Cl^-, NO_3^-, and Na^+ (Gomez and Martínez, 2010; Blarasin et al., 2020). In general, the correlation between NO_3^-/Na^+ and Cl^-/Na^+ can be used to evaluate the impacts of human activities on NO_3^- components in groundwater or surface water (Dutta et al., 2016).

Figure 10A shows that there is a certain correlation between NO_3^-/Na^+ and Cl^-/Na^+ in the groundwater in the study area, and most of the sampling points are located in the areas affected by agricultural activities, indicating that agricultural production activities in the area have affected the hydrochemical components of the groundwater to a certain extent (Farooq et al., 2021). In general, agricultural activities result in relatively high NO_3^-/Ca^{2+} and low SO_4^{2-}/Ca^{2+} values, while mining activities have the opposite effects (Singh et al., 2006). It is clearly seen from Figure 10B that the water samples in the study area have low NO_3^-/Ca^{2+} values, and most of the samples are located in areas affected by agricultural activities, further confirming that the groundwater is significantly affected by agricultural activities.

Maintaining and improving the hydrochemical quality requires a multifaceted approach involving regular monitoring of the water for pH, dissolved oxygen, heavy metals, and pollutants; protecting water sources from industrial, agricultural, and residential pollution; implementing effective water treatment methods like filtration, disinfection, and advanced techniques; maintaining distribution systems to prevent contamination; educating the public on water conservation and safe disposal of hazardous materials; enforcing water quality standards and holding polluters accountable; investing in research for innovative water purification technologies; and encouraging community involvement in local water protection initiatives.

5.2 Health risk assessment of groundwater in the study area

Based on the groundwater quality evaluation results and by considering that nitrates in drinking water mainly enter the human body through skin contact and direct intake, NO_3^- was selected as the key index affecting the quality of shallow groundwater in the study area for health risk assessment. The nitrate health risk indexes of the study area are shown in Table 6 and Figure 11. The average $HQ_{skin\ contact}$ values of children, adult men, and adult women in the study area for skin contact with shallow groundwater were 1.941×10^{-4}, 9.704×10^{-5}, and 1.592×10^{-4}, respectively (Table 6), all of which were less than 1 (Figure 11A). This shows that the non-carcinogenic health risk of groundwater in the study area was extremely low under the condition of skin contact and exposure; this was also consistent with other findings reported in literature (Khan et al., 2021b).

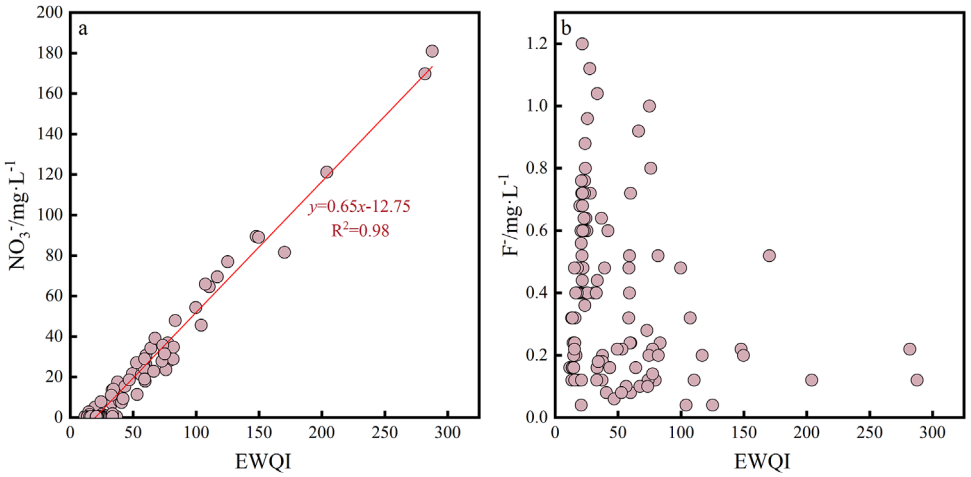

FIGURE 9
Scatter plots of the entropy-weighted water quality index (EWQI) against factors degrading the groundwater quality. Among them, **(A)** represents the relationship between EWQI and NO_3^- ions; while **(B)** represents the relationship between EWQI and F^- ions.

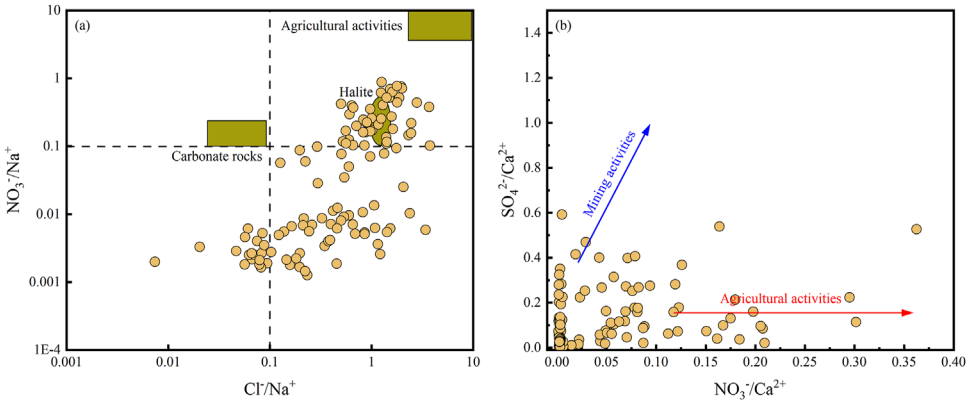

FIGURE 10
Relationships of **(A)** NO_3^-/Na^+ vs. Cl^-/Na^+ and **(B)** SO_4^{2-}/Ca^{2+} vs. NO_3^-/Ca^{2+} in groundwater and surface water in the study area.

TABLE 6 Non-carcinogenic risks of nitrate for drinking water intake and dermal contact.

Classification	Drinking water intake risk index (HQ)		Skin contact risk index (HQ)		Total risk index (HI)	
	Range	Mean	Range	Mean	Range	Mean
Children	0.009–3.393	0.354	2.137×10^{-4} to 1.859×10^{-3}	1.941×10^{-4}	9.380×10^{-3} to 3.395	3.544×10^{-1}
Adult female	0.008–3.009	0.314	2.568×10^{-6} to 9.296×10^{-4}	9.704×10^{-5}	8.315×10^{-3} to 3.010	3.141×10^{-1}
Adult male	0.009–3.329	0.329	4.215×10^{-6} to 1.526×10^{-4}	1.592×10^{-4}	8.706×10^{-3} to 3.151	3.289×10^{-1}

Chronic daily intake (CDI) in children and adults is mainly related to the drinking water rate (IR), average weight (BW), and average exposure time (AT) parameters. From Equation 10, it is seen that the concentration of contaminants in water (Ci) is considered equal for both children and adults, but parameters like the IR, BW, and AT control the specific CDI amounts for children and adults. Therefore, the daily intake values of the target substances are different for children and adults.

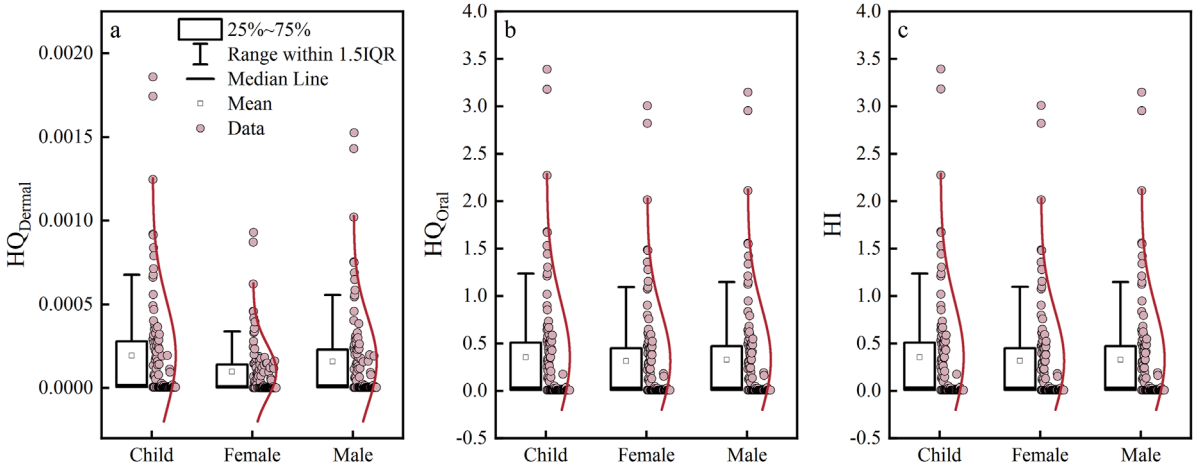

FIGURE 11
Box plots of the groundwater health risk indexes in the study area. Among them, **(A–C)** respectively represent the mathematical statistical results of HQ_{Demal}, HQ_{Oral}, and HI for children, males, and females.

The $HQ_{drinking\ water\ intake}$ risk indexes for children's drinking water exposure was between 0.009 and 3.393, with a mean of 0.354 (Figure 11B); adult women was between 0.008 and 3.009, with a mean of 0.314; and adult men was between 0.009 and 3.150, with a mean of 0.329. The risk index for drinking water exposure could be prioritized as children > adult men > adult women. Based on the risk index grade, 11 samples (10%) of children's HQ drinking water intake were greater than 1, while 10 samples (9.09%) were evaluated for both adult men and women with a drinking water intake risk of more than 1. Overall, the non-carcinogenic health risk of groundwater in the study area was small for drinking water intake as the exposure route.

Based on the total risk index, the average HI values of children, adult women, and adult men were 3.544×10^{-1}, 3.141×10^{-1}, and 3.289×10^{-1}, respectively (Table 6), showing that priority was children > adult men > adult women. Approximately 10% of the water samples in the study area showed a total risk index HI greater than 1 (Figure 11C), and these water samples were numbered FS011, FS023, FS064, FS074, FS087, FS097, FS130, FS136, FS137, FS340, and FS359, as shown in Figure 1. According to the verifications, shallow groundwater wells were drilled by the residents in parts of the study area to meet their drinking water needs, and the sampling points near these wells were close to ditches, vegetable gardens, and other areas with strong human activities. In addition, most of the wells were built in the 1990s with completed well depths of 5–15 m, so the well completion conditions were poor and greatly affected by external pollution. The health risk assessment results were consistent with the groundwater quality grade assessments, that is, water samples with poor groundwater quality grade had high non-carcinogenic health risks.

In conclusion, the important health implications within the study region stem from the consumption of drinking water and primarily affect the resident population, among which children represent the most sensitive segment, followed sequentially by adult men and women. This correlation underscores the urgent need for targeted interventions. The EWQI (Ukah et al., 2020; Kumar and Augustine, 2022) findings indicate that the bulk of the groundwater in the target shallow aquifers of the coalfield is of good to excellent quality. However, there is notable concern regarding nitrates as the primary indicators of suboptimal water quality, albeit the associated risks of nitrate contamination within the groundwater system remain low and pose only a marginal threat to general human health. Nonetheless, the elevated risk index specific to children's health compared to that of adults necessitates greater vigilance. This disparity underscores the vulnerability of this demographic to waterborne contaminants, warranting strategic focus on intensifying groundwater nitrate monitoring programs. Given the global significance of coalfield hydrogeology and its intricate relationships with hydrochemistry and health risks, this recommendation is aligned with scholarly discourse and practical imperatives aimed at safeguarding public health under these unique geological settings.

Samal et al. (2022) evaluated the hydrogeochemical characteristics of a coal mining region in eastern India and presented the quality as well as potential health risk assessment results for the groundwater in the area. They contended that groundwater chemistry studies would contribute to understanding the impacts of coal mining on the region's water resources. Notably, they highlighted that the people residing in the coal mining areas experience higher health risks, with an astonishing 90% of the water samples having HI >1, far surpassing the 10% noted in the present current study, as depicted in Figure 11C. This non-carcinogenic risk is particularly alarming for children, as noted in our research. Furthermore, Neogi et al. (2017) conducted an in-depth study on the hydrogeochemical characteristics and performed water quality assessments of the coal mine water in the North Karanpura Coalfield in India, concluding that the coal mine water was unsuitable for direct consumption and household use and that treatment prior to utilization was necessary.

6 Conclusion

The hydrochemical signatures of shallow groundwater within coalfields exhibit broad diversity and intricacy globally, which intricately stem from the interplay between geological formations, climatic variabilities, and anthropogenic influences. This intricate tapestry results in pronounced regional disparities with regard to ion types, trace element concentrations, and pollutant loads present in these aquifers. Our research focuses on the coalfield expansion in Huainan, Anhui Province, China, and meticulously unravels the ramifications of such developments on the hydrochemical profiles of groundwater and consequent health hazards to the local population. We conclusively establish that potable water consumption is the primary conduit of human exposure to altered groundwater conditions. Intriguingly, our findings underscore the potential for carcinogenic health threats from heavy metal contamination of drinking water, with nitrate pollution emerging as a particularly pernicious contributor to this risk landscape. This analysis not only contributes to the ongoing discourse among international scholars on the hydrochemistry of coalfield-associated shallow groundwater but also underscores the urgency for targeted risk assessments and mitigation measures to safeguard public health in the face of evolving environmental challenges.

(1) Groundwater within the study region exhibited a weakly alkaline nature dominated by HCO_3^- and Ca^{2+} ions, indicative of the predominant influence of rock weathering processes. The primary hydrochemical type was HCO_3-Ca that was closely followed by HCO_3-Ca·Na, reflecting a gradual evolution from Cl-Ca·Na to HCO_3-Ca·Mg and ultimately HCO_3-Na, underscoring the dynamic nature of groundwater chemistry in coalfield shallow aquifers.

(2) The analysis revealed SI values exceeding 0 for calcite, dolomite, and fluorite, suggesting their deposition and precipitation. Gypsum was noted to maintain a state of dissolution equilibrium, while halite exhibited intense dissolution. The inverse hydrogeochemical modeling revealed congruent evolutionary trajectories between paths I and IV that were largely dictated by Ca^{2+} dissolution–precipitation dynamics and cation-exchange adsorption. Conversely, paths II and III shared similar evolutionary patterns that were primarily steered by calcium montmorillonite precipitation as well as kaolinite, calcite, and quartz dissolution alongside heterogeneous minerals, underscoring the intricate interplay between geochemical processes in shaping groundwater chemistry.

(3) Assessments using the EWQI demonstrated that a substantial proportion (65.45%) of groundwater samples belonged to Grade 1 and Grade 2 categories, indicative of excellent to good water quality. However, a quarter (25.55%) of the samples were deemed to be of poor quality, and a minor portion (3.64%) was classified as Grade 5, highlighting the need for attention. Notably, NO_3^- was found to be the primary contributor to water quality degradation.

(4) With regard to human health implications, drinking water intake was identified as the primary exposure route in the study area. The evaluation of potential non-carcinogenic risks revealed a clear hierarchy among different age and gender groups, with children having the highest risk, followed by adult men and adult women. Although the overall risk index for nitrate pollution of groundwater remained low, posing minimal threat to human health, its disproportionate impact on children's health underscores the necessity for heightened vigilance and targeted mitigation measures, particularly in the context of coalfield shallow groundwater systems, which are the focus of ongoing research and discourse among international scholars.

(5) Coal resources are ubiquitous across the globe, albeit with pronounced regional imbalances. Nevertheless, the global distribution of proven coal reserves remains relatively balanced, with nearly 80 countries like China, the United States, Russia, India, Indonesia, Australia, and South Africa being notably endowed with this resource. This global dispersion of coal resources is the basis for economic growth in various nations. However, coal extraction significantly impacts the groundwater in mining regions and is responsible for direct water loss, water quality deterioration, water table decline, disruption of the hydrological cycle, and potential geohazards. Critically, these consequences may ultimately jeopardize potable water supply for the local population, thereby affecting human health. Hence, it is imperative to enhance our understanding of hydrological environments and the chemical processes influencing groundwater in coal mining areas. Such knowledge would then facilitate the long-term conservation and efficient management of water resources while preemptively mitigating the health risks associated with coal mining operations in these regions.

Data availability statement

The original contributions presented in this study are included in the article/supplementary material, and any further inquiries may be directed to the corresponding author.

Author contributions

JS: writing–original draft, writing–review and editing. XZ: writing–original draft, writing–review and editing.

Funding

The authors declare that financial support was received for the research, authorship, and/or publication of this article. This work received financial support from the Anhui Provincial Key Research and Development Programs (No. 2022n07020003).

Conflict of interest

Author XZ was employed by Sino-Pipeline International Company.

The remaining author declares that the research was conducted in the absence of any commercial or financial relationships that could be construed as a potential conflict of interest.

Publisher's note

All claims expressed in this article are solely those of the authors and do not necessarily represent those of their affiliated organizations or those of the publisher, editors, and reviewers. Any product that may be evaluated in this article or claim that may be made by its manufacturer is not guaranteed or endorsed by the publisher.

References

Addis, Z. (2023). Assessment of groundwater hydrochemistry using multivariate statistical analysis techniques and aquachem (piper trilinear) the case study of wabishable basin, Ethiopia. *J. Water Res.* 1 (2), 82–98. doi:10.33140/jwr.01.02.03

Aliejin, O. A. (1960). *Hydrographic chemical principles. Translated by Zhang Z Y.* Beijing: Geological Publishing House.

Ambade, B., Sethi, S. S., Kurwadkar, S., Kumar, A., and Sankar, T. K. (2021). Toxicity and health risk assessment of polycyclic aromatic hydrocarbons in surface water, sediments and groundwater vulnerability in Damodar River Basin. *Groundw. Sustain. Dev.* 13, 100553. doi:10.1016/j.gsd.2021.100553

Andres, M., and Paul, S. (2018). Groundwater chemistry and the Gibbs diagram. *Appl. Geochem.* 97, 209–212. doi:10.1016/j.apgeochem.2018.07.009

Bakshe, P., Chandran, M., Viju, B. J., Narikkatan, A. K., and Jugade, R. M. (2024). Hydrogeochemical factors influencing the dynamics of groundwater characteristics in eco-sensitive areas of the Southern Western Ghats, India. *Sci. Rep.* 14 (1), 19143. doi:10.1038/s41598-024-67988-6

Blarasin, M., Cabrera, A., Matiatos, I., Becher Quinodóz, F., Giuliano Albo, J., Lutri, V., et al. (2020). Comparative evaluation of urban versus agricultural nitrate sources and sinks in an unconfined aquifer by isotopic and multivariate analyses. *Sci. Total Environ.* 741, 140374. doi:10.1016/j.scitotenv.2020.140374

Chai, Y. L. (2018). Discussion on assessment method of mine geo-environment impact in the Huainan mining area. *Geol. Anhui* 28 (4), 299–302. doi:10.1016/j.scitotenv.2020.140374

Du, S. D., Guan, Y. N., Li, X., Zhao, Y. Q., Liu, S. J., Yan, C. Y., et al. (2022). Water quality evaluation with improved comprehensive pollution index based on entropy weight Method: a case study of Baiyun Lake. *Acta Sci. Circumstantiae* 42 (1), 205–212. doi:10.13671/j.hjkxxb.2021.0108

Dutta, S., Gogoi, R., Rashmi, Khanikar, L., Bose, S., Rajat, P., et al. (2016). Assessment of hydrogeochemistry and water quality index (WQI) in some wetlands of the Brahmaputra valley, Assam, India. *Desalination Water Treat.*, 1–13. doi:10.1080/19443994.2016.1177598

El Ghali, T., Marah, H., Qurtobi, M., Raibi, F., Bellarbi, M., Amenzou, N., et al. (2020). Geochemical and isotopic characterization of groundwater and identification of hydrogeochemical processes in the Berrechid aquifer of central Morocco. *Carbonates Evaporites* 35 (2), 37. doi:10.1007/s13146-020-00571-y

Fan, B. L., Zhao, Z. Q., Tao, F. X., Liu, B. J., Gao, S., Zhang, L. H., et al. (2014). Characteristics of carbonate, evaporite and silicate weathering in Huanghe River basin: a comparison among the upstream, midstream and downstream. *J. Asian Earth Sci.* 96 (15), 17–26. doi:10.1016/j.jseaes.2014.09.005

Farooq, U., Choudhary, B., Sen, I., Bowes, M., Glendell, M., Ray, S., et al. (2021). Understanding water pollution and its pathways in the ramganga river basin, India using multi-source datasets. *AGU Fall Meet. Abstr.* 2021. Available at: https://ui.adsabs.harvard.edu/abs/2021AGUFM.H25W1289F/abstract.

Gaillardet, J., Dupré, B., Louvat, P., and Allègre, C. (1999). Global silicate weathering and CO_2 consumption rates deduced from the chemistry of large rivers. *Chem. Geol.* 159 (1-4), 3–30. doi:10.1016/S0009-2541(99)00031-5

Gao, S., Li, C. S., Jia, C., Zhang, H., Guan, Q., Wu, X., et al. (2020). Health risk assessment of groundwater nitrate contamination: a case study of a typical karst hydrogeological unit in East China. *Environ. Sci. Pollut. Res.* 27, 9274–9287. doi:10.1007/s11356-019-07075-w

Gibbs, R. J. (1970). Mechanisms controlling world water chemistry. *Science* 17 (3962), 1088–1090. doi:10.1126/science.170.3962.1088

Gomez, M. L., and Martínez, D. E. (2010). Municipal waste management and groundwater contamination processes in Córdoba Province, Argentina. *Ambiente e Agua-An Interdiscip. J. Appl. Sci.* 5 (3), 28–46. doi:10.4136/ambi-agua.152

Groundwater quality standard (2017). *Ministry of Land and resources of the people's Republic of China, Ministry of water resources of the people's Republic of China. Groundwater quality standard GB/T 14848-2017*. Beijing: General Administration of Quality Supervision.

Huang, W. W., Jiang, C. L., Chen, X., Fu, X. J., Chen, S. G., Zheng, L. G., et al. (2020). Chemical characteristics and genesis of deep groundwater in the Xinji mining area. *Earth Environ.* 48 (4), 432–442. doi:10.14050/j.cnki.1672-9250.2020.48.075

Khan, U., Faheem, H., Jiang, Z., Wajid, M., Younas, M., and Zhang, B. (2021a). Integrating a GIS-based multi-influence factors model with hydro-geophysical exploration for groundwater potential and hydrogeological assessment: a case study in the Karak Watershed, Northern Pakistan. *Water* 13 (9), 1255. doi:10.3390/w13091255

Khan, Y. K., Toqeer, M., and Shah, M. H. (2021b). Spatial distribution, pollution characterization and health risk assessment of selected metals in groundwater of Lahore, Pakistan. *Geochemistry* 81 (1), 125692. doi:10.1016/j.chemer.2020.125692

Kim, S. H., Kim, H. R., Yu, S., Kang, H. J., Hyun, I. H., Song, Y. C., et al. (2021). Shift of nitrate sources in groundwater due to intensive livestock farming on Jeju Island, South Korea: with emphasis on legacy effects on water management. *Water Res.* 191, 116814. doi:10.1016/j.watres.2021.116814

Kumar, P. J., and Augustine, C. M. (2022). Entropy-weighted water quality index (EWQI) modeling of groundwater quality and spatial mapping in Uppar Odai Sub-Basin, South India. *Model. Earth Syst. Environ.* 8 (1), 911–924. doi:10.1007/s40808-021-01132-5

Li, W., Chen, X., Xie, L., Cheng, G., Liu, Z., and Yi, S. (2020). Natural and human-induced factors controlling the phreatic groundwater geochemistry of the Longgang River basin, South China. *Open Geosci.* 12 (1), 203–219. doi:10.1515/geo-2020-0039

Li, Z., Xiao, J., Evaristo, J., and Li, Z. (2019a). Spatiotemporal variations in the hydrochemical characteristics and controlling factors of streamflow and groundwater in the Wei River of China. *Environ. Pollut.* 254, 113006. doi:10.1016/j.envpol.2019.113006

Li, Z. J., Yang, Q. C., Yang, Y. S., Ma, H., Wang, H., Luo, J., et al. (2019b). Isotopic and geochemical interpretation of groundwater under the influences of anthropogenic activities. *J. Hydrogeology* 576, 685–697. doi:10.1016/j.jhydrol.2019.06.037

Liu, H., Kamg, B., and Shen, J. H. (2019). Formation of groundwater based on inverse geochemical modeling: a case study from the Sixian county, Anhui province. *Geoscience* 33 (02), 440–450. doi:10.19657/j.geoscience.1000-8527.2019.02.19

Liu, M. J., Xiao, C. L., Liang, X. J., and Wei, H. (2022). Response of groundwater chemical characteristics to land use types and health risk assessment of nitrate in semi-arid areas: a case study of Shuangliao City, Northeast China. *Ecotoxicol. Environ. Saf.* 236, 113473. doi:10.1016/j.ecoenv.2022.113473

Meng, Q. (2021). Hydrochemical characteristics and controlling factors of the shallow groundwater in the midstream and downstream of Shiyang river basin. *J. Land Resour. Enviroment* 35 (3), 80–87. doi:10.13448/j.cnki.jalre.2021.072

Mondal, D., Ghosh, S., Naveen, P., Kumar, M., Majumder, A., and Kumar Panda, A. (2021). An integrated study on the geochemical, geophysical and geomechanical characteristics of the organic deposits (Coal and CBM) of eastern Sohagpur coalfield, India. *Gondwana Res.* 96, 122–141. doi:10.1016/j.gr.2021.03.016

Neogi, B., Singh, A. K., Pathak, D. D., and Chaturvedi, A. (2017). Hydrogeochemistry of coal mine water of North Karanpura coalfields, India: implication for solute acquisition processes, dissolved fluxes and water quality assessment. *Environ. Earth Sci.* 76, 489. doi:10.1007/s12665-017-6813-4

Olea-Olea, S., Silva-Aguilera, R. A., Alcocer, J., Escolero, O., Morales-Casique, E., Florez-Peñaloza, J. R., et al. (2024). Water–rock interaction processes in groundwater and flows in a maar lake in Central Mexico. *Water* 16 (5), 715. doi:10.3390/w16050715

Piper, A. M. (1944). A graphic procedure in the geochemical interpretation of water-analyses. *Eos, Trans. Am. Geophys. Union* 25 (6), 914–928. doi:10.1029/TR025i006p00914

Prathap, A., and Chakraborty, S. (2019). Hydrochemical characterization and suitability analysis of groundwater for domestic and irrigation uses in open cast coal mining areas of Charhi and Kuju, Jharkhand, India. *Groundw. Sustain. Dev.* 9, 100244. doi:10.1016/j.gsd.2019.100244

Rashid, S., Shah, I. A., Supe Tulcan, R. X., Rashid, W., and Sillanpaa, M. (2022). Contamination, exposure, and health risk assessment of Hg in Pakistan: a review. *Environ. Pollut.* 301, 118995. doi:10.1016/j.envpol.2022.118995

Sahoo, S., and Khaoash, S. (2020). Impact assessment of coal mining on groundwater chemistry and its quality from Brajrajnagar coal mining area using indexing models. *J. Geochem. Explor.* 215, 106559. doi:10.1016/j.gexplo.2020.106559

Samal, P., Mohanty, A. K., Khaoash, S., and Mishra, P. (2022). Hydrogeochemical evaluation, groundwater quality appraisal, and potential health risk assessment in a coal mining region of Eastern India. *Water, Air, & Soil Pollut.* 233 (8), 324. doi:10.1007/s11270-022-05811-6

Singh, S. P., Khare, P., Kumari, K. M., and Srivastava, S. (2006). Chemical characterization of dew at a regional representative site of North-Central India. *Atmos. Res.* 80 (4), 239–249. doi:10.1016/j.atmosres.2005.09.003

Tomiyama, S., and Igarashi, T. (2022). The potential threat of mine drainage to groundwater resources. *Curr. Opin. Environ. Sci. & Health* 27, 100347. doi:10.1016/j.coesh.2022.100347

Ukah, B. U., Ameh, P. D., Egbure, J. C., Unigwe, C. O., and Ubido, O. E. (2020). Impact of effluent-derived heavy metals on the groundwater quality in Ajao industrial area,Nigeria: an assessment using entropy water quality index (EWQI). *Int. J. Energy Water Resour.* 4 (3), 231–244. doi:10.1007/s42108-020-00058-5

Wang, Z. T., Liu, Q. M., and Liu, Y. (2019). Spatial distribution and formation of groundwater hydrochemistry in Huainan coalfield. *Coal Geol. & Explor.* 47 (5), 40–47. doi:10.3969/j.issn.1001-1986.2019.05.006

WHO (2011). *Guideline for drinking-water quality*. 4th ed. Geneva: WHO.

Wu, J. H., Zhang, Y. X., and Zhou, H. (2020b). Groundwater chemistry and groundwater quality index incorporating health risk weighting in Dingbian County, Ordos basin of northwest China. *Geochemistry* 80 (4), 125607. doi:10.1016/j.chemer.2020.125607

Wu, T. H., Liu, H. Y., Zhang, W. M., Sun, Z. X., Wang, Z., and Liu, M. H. (2022). Hydrochemical characteristics and human health risk assessment in downstream Ganjiang river of the Poyang lake basin. *Geoscience* 36 (2), 427–438. doi:10.19657/j.geoscience.1000-8527.2022.018

Wu, X. J., Zhang, L., Hu, B. X., Wang, Y., and Xu, Z. (2020a). Isotopic and hydrochemical evidence for the salinity origin in the coastal aquifers of the Pearl River Delta, Guangzhou, China. *J. Contam. Hydrology* 235, 103732. doi:10.1016/j.jconhyd.2020.103732

Xiao, Y., Hao, Q. C., Zhang, Y. H., Zhu, Y., Yin, S., Qin, L., et al. (2021). Investigating sources, driving forces and potential health risks of nitrate and fluoride in groundwater of a typical alluvial fan plain. *Sci. Total Environ.* 802, 149909. doi:10.1016/j.scitotenv.2021.149909

Xu, G. Q., Liu, J., and Zhu, Q. S. (2009). Analysis of distribution characteristics and influencing factors for the fluorine in the shallow groundwater in Huaibei plain of Anhui. *J. Water Resour. & Water Eng.* 20 (5), 9–13.

Yan, J., Chen, J., and Zhang, W. (2021). Study on the groundwater quality and its influencing factor in Songyuan City, Northeast China, using integrated hydrogeochemical method. *Sci. Total Environ.* 773, 144958. doi:10.1016/j.scitotenv.2021.144958

Yang, T. T., Xu, G. Q., and Anesu, M. (2021). Chemical composition of karst groundwater of panxie coal mining area in Huainan and its formation mechanism. *Earth Environ.* 49 (3), 238–249. doi:10.14050/j.cnki.1672-9250.2021.49.024

Zhang, J., Li, Y. S., Lin, M. L., Sun, L. H., Du, Z. L., and Li, J. (2014). Hydrogeochemistry characteristics and source identification: a case study in the Zhangji coal mine in Huainan. *Hydrogeology & Eng. Geol.* 41 (6), 32–37.

Zhang, Y. T., Wu, J. H., and Xu, B. (2018). Human health risk assessment of groundwater nitrogen pollution in Jinghui canal irrigation area of the loess region,northwest China. *Environ. Earth Sci.* 77 (7), 273–312. doi:10.1007/s12665-018-7456-9

Zineb, A., and Meriem, L. (2024). Formation mechanism of hydrochemical and quality evaluation of shallow groundwater in the Upper Kebir sub-basin, Northeast Algeria. *J. Groundw. Sci. Eng.* 12 (1), 78–91. doi:10.26599/jgse.2024.9280007

Zipper, C. E., and Skousen, J. (2021). Coal's legacy in Appalachia: lands, waters, and people. *Extr. Industries Soc.* 8 (4), 100990. doi:10.1016/j.exis.2021.100990